Journal of Photochemistry and Photobiology A: Chemistry 289 (2014) 22–30

Contents lists available at ScienceDirect

Journal of Photochemistry and Photobiology A: Chemistry

journal homepage: www.elsevier.com/locate/jphotochem

Visible-light-absorbing mesoporous TiO_2 modified with tungstosilicic acid as photocatalyst in the photodegradation of 4-chlorophenol

Julián A. Rengifo-Herrera*, Romina A. Frenzel, Mirta N. Blanco, Luis R. Pizzio*

Centro de Investigación y Desarrollo en Ciencias Aplicadas "Dr. J. J. Ronco" (CINDECA), Departamento de Química, Facultad de Ciencias Exactas, UNLP-CCT La Plata, CONICET, 47 N° 257, 1900 La Plata, Argentina

ARTICLE INFO

Article history:
Received 13 January 2014
Received in revised form 19 May 2014
Accepted 23 May 2014
Available online 2 June 2014

Keywords:
Mesoporous titania
Tungstosilicic acid
4-Chlorophenol
Photocatalytic degradation

ABSTRACT

Visible-light-absorbing materials based on TiO_2 modified with tungstosilicic acid (TSA; $H_4SiW_{12}O_{40}$) were prepared using titanium isopropoxide as precursor and urea as a low-cost pore-forming agent. X-ray diffraction (XRD) measurements show evidence about the presence of anatase TiO_2 in all samples and shifting of the anatase–rutile transition temperature toward temperatures higher than 600 °C. The FT-IR and FT-Raman studies showed that the main heteropolyoxometallate species present in the composites annealed up to 500 °C is the $[SiW_{12}O_{40}]^{4-}$ anion, which exhibited a strong interaction with TiO_2 surface probably due to the formation of TSA–TiO_2 complexes that should be responsible for its visible light absorption. The photocatalytic activity of these materials was tested using 4-chlorophenol as model pollutant. Results revealed that photocatalytic activity mainly depends on the TSA amount and the annealing temperature. The amount of degraded 4-CP increased with the increment of TSA content, with the one calcined at 600 °C being more active. Finally, it was found that these photocatalysts can be reused at least three times without an important decrease in the degradation and mineralization degrees.

1. Introduction

In the last twenty years, photocatalytic oxidation processes using TiO_2 have been considered as a promising alternative to destroy a wide range of waterborne pollutants and microorganisms [1–3]. However, TiO_2 photocatalysis still today has two big drawbacks to overcome. The first one is the high recombination of photo-induced electron–hole pairs, since around 90% of charge carriers undergo fast recombination in the range of nanoseconds [4]; the second one is related to the light absorption of TiO_2 since it is well known that this semiconductor absorbs only UV light limiting its application in solar-driven processes [5].

Different strategies have been reported in the literature to overcome these limitations. For instance, to decrease the fast electron–hole recombination, the addition of noble metals such as platinum and silver has been successfully explored. Noble metals act as a sink of conduction band photo-induced electrons avoiding their recombination and enhancing the photocatalytic process [6]. On the other hand, to increase the TiO_2 light absorption toward the visible region (the wavelengths more abundant on the planet's surface), different efforts have been made. Doping with metal and nonmetal elements has risen as a successful strategy to prepare visible-light-absorbing TiO_2 [5,7–9]; however, the photocatalytic activity of these materials in the degradation of waterborne pollutants, especially N-doped TiO_2, is not high since during visible light irradiation these materials could yield reactive oxygen species with lower power oxidation [10,11].

Heteropolyoxometallates (POMs) are clusters of transition metals and oxygen that are widely used as oxidation as well as acid catalysts [12–14]. POMs such as tungstosilicic acid (TSA) have often been used as effective homogeneous photocatalysts in the oxidation of organic compounds [15] and in the degradation of organic pollutants in water [16]. It has been demonstrated that the incorporation of POMs such as tungstophosphoric acid ($H_3PW_{12}O_{40}$, TPA) into TiO_2 leads to visible-light-absorbing materials with high photocatalytic activity [17–20]. The latter is due to the fact that TPA on the TiO_2 surface acts as an effective trap of photo induced electrons decreasing the fast e^-/h^+ recombination [21]. Visible light absorption of TiO_2 modified with TPA could be due to the formation of a surface complex between the Keggin structure of TPA and the TiO_2 surface or to the formation of Keggin–TPA/TiO_2 composites [17,19]. To our knowledge, there are only two studies reported in the literature about the modification of TiO_2 by tungstosilicic acid (TSA) and its application to the destruction of waterborne pollutants [22,23].

* Corresponding authors. Tel.: +54 221 421 1353; fax: +54 221 425 4477.
E-mail addresses: julianregifo@quimica.unlp.edu.ar (J.A. Rengifo-Herrera), lrpizzio@quimica.unlp.edu.ar (L.R. Pizzio).

http://dx.doi.org/10.1016/j.jphotochem.2014.05.014
1010-6030/

In the present work, we synthesized, by the sol–gel method, mesoporous TiO_2 nanospheres modified with different amounts of tungstosilicic acid (10, 20, and 30% w/w) and extended the temperature range of treatment of the materials to temperatures higher than 600 °C. The photocatalytic activity of these materials toward the oxidation of 4-chlorophenol was evaluated. Finally, we discuss the effect of the preparation variables on the structural and textural characteristics of the solids and correlate them with the pollutant degradation activity.

2. Materials and methods

2.1. Synthesis of TSA/titania composites

A titanium isopropoxide (Aldrich, 26.7 g) solution was prepared in absolute ethanol (Merck, 186.6 g) under N_2 atmosphere and at room temperature, continuously stirring for 10 min. Then, 0.33 cm^3 of a 0.28 M HCl aqueous solution was slowly added in order to catalyze the sol–gel reaction. After 3 h, 120 g of a urea–ethanol–water (1:5:1 weight ratio) solution was added, together with an ethanol solution of tungstosilicic acid ($H_4SiW_{12}O_{40}{\cdot}23H_2O$, Fluka p.a.) under vigorous stirring. The amount of TSA was varied with the purpose of obtaining a TSA concentration of 0%, 10%, 20% and 30% by weight in the final solid (named TiTSA00, TiTSA10, TiTSA20, and TiTSA30, respectively). The gels were dried at room temperature, and the solids were ground into powder and extracted with distilled water for three periods of 24 h, in order to remove the urea. Finally, the solids were thermally treated at 100, 500, 600, 700 and 800 °C for 2 h ($TiTSAXX_{T100}$, $TiTSAXX_{T500}$, $TiTSAXX_{T600}$, $TiTSAXX_{T700}$, and $TiTSAXX_{T800}$, respectively, where XX is the TSA concentration).

The W content on the TiTSAXX samples was estimated as the difference between the W amount contained in the tungstosilicic acid ethanol solution originally added and the amount of W released during urea extraction. The amount of W in the water solutions obtained after the ground solids were extracted was determined by atomic absorption spectrometry using a Varian AA Model 240 spectro-photometer. The calibration curve method was used with standards prepared in the laboratory. The analyses were carried out at a wavelength of 254.9 nm, bandwidth 0.3 nm, lamp current 15 mA, phototube amplification 800 V, burner height 4 mm, and acetylene–nitrous oxide flame (11:14). The results obtained reveal that the W contents in the samples were 9.8%, 19.7% and 29.5% (w/w) for TiTSA10, TiTSA20, and TiTSA30, respectively.

2.2. Sample characterization

The specific surface area, the pore volume and the mean pore diameter of the solids were determined from the N_2 adsorption–desorption isotherms at the liquid-nitrogen temperature, obtained using Micromeritics ASAP 2020 equipment. The solids were previously degassed at 100 °C for 2 h. The specific surface area (S_{BET}) of the samples was determined using the BET method, the specific surface area of micropores (S_{micro}) was estimated by the *t*-plot method, and the average pore diameter (D_p) was obtained using the Barret–Joyner–Halenda (BJH) method.

The X-ray diffraction (XRD) patterns were recorded with Philips PW-1732 equipment with a built-in recorder, using Cu Kα radiation, nickel filter, 20 mA and 40 kV in the high voltage source, and scanning angle between 5° and 60° 2θ at a scanning rate of 1°/min. The crystallite size (D_C) of the samples was estimated from the XRD results using the Scherrer equation and silicon as standard for the correction of the instrumental broadening.

The Fourier transform infrared (FT-IR) spectra of the solids were obtained using a Bruker IFS 66 FT-IR spectrometer and pellets in KBr in the 400–4000 cm^{-1} wavenumber range. Fourier transform Raman scattering (FT-Raman) spectra were recorded on a Raman Horiba Jobin-Yvon T 64000 instrument with an Ar^+ laser source of 488 nm wavelength in a macroscopic configuration.

The diffuse reflectance spectra (DRS) of the materials were recorded using a UV-visible Lambda 35, Perkin Elmer spectrophotometer, to which a diffuse reflectance chamber Labsphere RSA-PE-20 with an integrating sphere of 50 mm diameter and internal Spectralon coating is attached, in the 200–800 nm wavelength range. The *band gap* values (E_g) were estimated from the corresponding Kubelka–Munk remission functions, calculated from the absorbance values of the DRS spectra.

2.3. Photodegradation reaction

The catalytic activity of the mesoporous TiO_2 spherical nanoparticles modified with tungstosilicic acid was evaluated in the photodegradation of 4-chlorophenol (Fluka) in water, at 25 °C. The tests were carried out employing a 125 W high-pressure mercury lamp (with a maximum emission at about 365 nm) placed inside a Pyrex glass jacket, thermostated by water circulation, and immersed in the 4-chlorophenol (4-CP) solution contained in a 300 ml cylindrical Pyrex glass reactor. The catalyst was maintained in suspension by stirring, and air was continuously bubbled. Previously, the 4-CP solution (200 ml, 1.5×10^{-4} mol/l) containing 100 mg of catalyst was magnetically stirred in the absence of light for 60 min to ensure that the adsorption–desorption equilibrium of 4-CP on the surface of the materials was attained. The pH of the experiments was 6.9.

Samples (3 ml) taken at different illumination times were filtered through membranes of 0.45 μm pore size, and measured by UV–vis spectrophotometry (Lambda 35-Perkin-Elmer) monitoring the absorbance at 255 nm. All the measurements were carried out three times.

The filtrates were extracted three times with ethyl ether, the organic layers were collected, dried with sodium sulfate, and concentrated for the determination of the intermediates using a Hewlett Packard 6890N GC/MSD.

The extent of 4-CP mineralization was determined using the Total Organic Carbon, Method 10129 DR/4000 (HACH).

In order to evaluate the possibility of TSA leaching during the photocatalytic degradation of 4-CP, at the end of each experiment, the catalyst was separated by decantation, and W was determined in the liquid phase by atomic absorption spectrometry using a Varian AA Model 240 spectrophotometer and the above-mentioned technique.

The catalytic activity of the materials was compared with commercially available titania P25 Degussa measured under the same experimental conditions.

3. Results and discussion

3.1. Sample characterization

3.1.1. X-ray diffraction (XRD)

According to the XRD patterns of $TiTSA00_{T100}$, $TiTSA10_{T100}$, $TiTSA20_{T100}$, and $TiTSA30_{T100}$ samples (data no shown), the solids are poorly crystallized and mostly amorphous.

In the XRD pattern of the $TiTSA00_{T500}$ samples, the peak at 54.3° is split into two peaks at 54.0° and 54.9°, corresponding to the (1 0 5) and (2 1 1) reflections of the anatase phase [24]. The XRD pattern of the $TiTSA00_{T600}$ sample exhibited three new peaks at 2θ = 27.4°, 36.1°, and 54.2°, as a result of the partial transformation of anatase into rutile phase. The transformation was complete for the TiTSA00 sample treated at higher temperatures, because only the

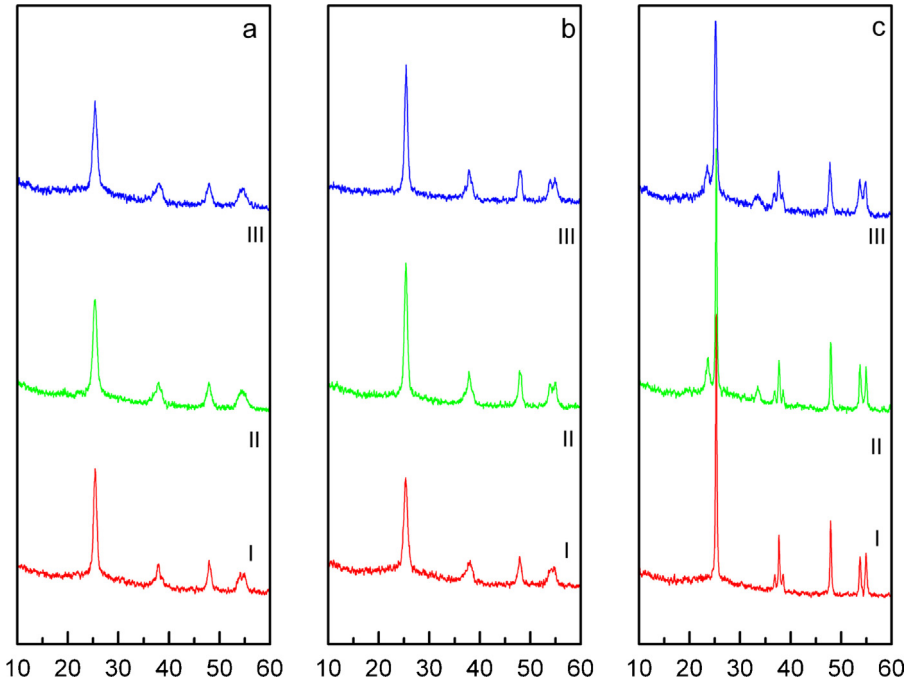

Fig. 1. XRD patterns of TiTSA10 (a), TiTSA20 (b), and TiTSA30 (c) samples calcined at 600 (I), 700 (II), and 800 °C (III).

characteristic peaks of the rutile phase are present in the XRD pattern of $TiTSA00_{T700}$ and $TiTSA00_{T800}$.

On the other hand, the XRD patterns of TiTSA10, TiTSA20, and TiTSA30 samples calcined at 600, 700, and 800 °C (Fig. 1a, b, c, respectively) showed only the presence of titania in an anatase-type structure, suggesting that the phase transition of anatase into rutile is shifted to higher temperatures in the presence of TSA. Additionally, the crystallinity increased when the calcination temperature was raised. However, the increment was lower for the samples with higher TSA content.

The samples with higher TSA content calcined at 800 °C ($TiTSA20_{T800}$ and $TiTSA30_{T800}$) also display two new broad peaks at $2\theta = 23.5^\circ$ and 33.5°, which could be assigned to the presence of small crystals resulting from the thermal decomposition of TSA [23] that takes place at temperatures higher than 500 °C.

The results showed that the presence of TSA retarded the crystallization of titania and stabilized TiO_2 in the anatase phase, in agreement with literature reports of titania modified with tungsten oxide [25,26].

As is generally reported, we observed that the crystallite size (D_C) of the samples (Tables 1 and 2) increases with the increment of the calcination temperature. However, the increment was lower for the samples with higher TSA content. This is a common behavior in materials containing both a crystalline and an amorphous phase [27] and it may be attributed to crystal growth delay.

3.1.2. Brunauer–Emmett–Teller (BET) specific surface area and textural features

The results for the TiTSA00 sample calcined at different temperatures are shown in Table 1.

From the average pore diameter (D_p) we can conclude that all the samples are mesoporous materials with a D_p higher than 3.1 nm (Tables 1 and 2). Their specific surface area (S_{BET}) decreased and the mean pore radius increased when the calcination temperature was raised from 100 to 800 °C.

According to the S_{BET} and S_{micro} values (Tables 1 and 2), only the $TiTSAXX_{T100}$ samples display micropores, though less than 10% of the total specific surface area is due to a microporous structure.

The S_{BET} values of the TSA-modified samples treated at 100 °C decrease in the following order: $TiTSA10_{T100} > TiTSA20_{T100} > TiTSA30_{T100}$ (Table 2), and are lower than the $TiTSA00_{T100}$ value. According to the literature, the lower S_{BET} values may be due to a decrease in the cross-linking degree when the acid concentration increases [28,29]. They are also in agreement with our previous reports on the specific surface area of mesoporous titania modified by the addition of TPA [30].

The S_{BET} of TSA-modified samples also decreased when the calcination temperature was increased (Table 2). However, the decrease of S_{BET} is lower for the samples with higher TSA content as a result of the strong interaction of TSA and the titania matrix, which reduces the surface diffusion of titania, and inhibits sintering [31–33].

Table 1
Physicochemical properties of the TiTSA00 sample treated at different temperatures.

Sample	S_{BET} (m^2/g)	S_{micro} [a] (m^2/g)	D_p [b] (nm)	D_c [c] (nm)		E_g (eV)	pH_{PZC} [d]
				Anatase	Rutile		
$TiTSA00_{T100}$	372	35	3.1	5.9	–	3.20	6.5
$TiTSA00_{T500}$	56	–	6.1	13.3	–	3.10	5.9
$TiTSA00_{T600}$	21	–	13.1	20.9	6.1	2.99	5.7
$TiTSA00_{T700}$	5	–	13.9	–	22.3	3.00	5.6
$TiTSA00_{T800}$	3	–	14.2	–	23.4	2.99	5.6

[a] Specific surface area of micropores obtained from *t*-plot analysis.
[b] Average pore diameter calculated using the BJH formula from the desorption branch.
[c] Scherrer crystallite size estimated using the characteristic anatase (1 0 1) and rutile (1 1 0) diffraction planes.
[d] From Ref. [28].

Table 2
Physicochemical properties of TSA/titania composites treated at different temperatures.

Sample	S_{BET} (m^2/g)	S_{micro}[a] (m^2/g)	D_p[b] (nm)	D_c[c] (nm) Anatase	E_g (eV)	pH_{PZC}[d]
$TiTSA10_{T100}$	238	18	4.2	5.5	3.00	6.1
$TiTSA20_{T100}$	208	15	4.8	5.5	2.97	6.0
$TiTSA30_{T100}$	160	12	5.0	5.6	2.95	5.4
$TiTSA10_{T500}$	87	–	4.9	9.8	2.95	5.2
$TiTSA20_{T500}$	115	–	4.1	8.1	2.93	4.2
$TiTSA30_{T500}$	118	–	4.3	7.9	2.90	2.9
$TiTSA10_{T600}$	63	–	9.4	12.3	2.90	5.1
$TiTSA20_{T600}$	82	–	7.6	9.2	2.86	4.1
$TiTSA30_{T600}$	83	–	7.3	8.8	2.85	2.9
$TiTSA10_{T700}$	29	–	15.1	20.7	2.90	5.1
$TiTSA20_{T700}$	42	–	16.3	13.5	2.88	4.0
$TiTSA30_{T700}$	47	–	13.5	9.2	2.86	2.8
$TiTSA10_{T800}$	22	–	16.7	21.8	2.90	5.0
$TiTSA20_{T800}$	31	–	17.9	18.6	2.88	4.0
$TiTPA30_{T800}$	35	–	14.6	12.0	2.87	2.8

[a] Specific surface area of micropores obtained from *t*-plot analysis.
[b] Average pore diameter calculated using the BJH formula from the desorption branch.
[c] Scherrer crystallite sizes estimated using the characteristic anatase (1 0 1) diffraction plane.
[d] From Ref. [22].

3.1.3. FT-IR and FT-Raman characterization

From the FT-IR studies previously reported [34], we established that the main species present in TiO_2 modified with TSA is the $[SiW_{12}O_{40}]^{4-}$ anion that remains unchanged during the subsequent thermal treatment up to 500 °C. However, the spectra of the samples treated at 600 °C and higher temperatures display a decrease in the intensity of the bands assigned to the anion (Fig. 2), possibly as a result of a partial degradation of the Keggin-type structure.

FT-Raman spectra of pristine TiO_2, bulk TSA, and $TiTSA20\text{-}30_{500}$, $TiTSA20\text{-}30_{600}$ were recorded and are shown in Fig. 3a. Anatase TiO_2 belongs to the tetragonal space group $D_{4h}{}^{1g}$ ($I4_1/amd$), which exhibits six Raman active modes ($A_{1g} + 2B_{1g} + 3E_g$) at 141.3 cm^{-1} (E_g), 394.4 cm^{-1} (B_{1g}), 516.1 cm^{-1}, (A_{1g}, B_{1g}), and 636.7 cm^{-1} (E_g) [35,36]. Fig. 3a shows the Raman spectrum of pristine TiO_2 revealing four bands at 141, 393, 515 and 636 cm^{-1} that agree very well with anatase TiO_2 phase. On the other hand, the FT-Raman spectrum of bulk TSA showed Raman vibration bands typically assigned to the Keggin anion at 1002, 980, 922, 881, and 787 cm^{-1}, which are attributed to antisymmetric and symmetric vibrations of W–O and W–O–W bonds [37,38]. Figs. 3a and 4b also show the Raman spectra of $TiTSA20\text{-}30_{500}$ and $TiTSA20\text{-}30_{600}$ samples revealing a broad peak at 950–1000 cm^{-1}; this broadening has also been reported for TiO_2 materials modified with tungstophosphoric acid and could be due to strong interactions between the Keggin anion of the heteropolyoxometallate [20,38]. In addition, Fig. 3c shows that the main Raman band of anatase TiO_2 at 141 cm^{-1} underwent an intensity decrease, broadening and strong blue shifting (shifting to higher wavenumber) in the samples containing TSA. This blue shifting is often related to phonon confinement, particle size reduction, deviations from stoichiometry, presence of oxygen vacancies or disorders induced by minority phases [35,36,39–41]. However, some authors have suggested that this blue shifting should be related to a strong interaction of the Keggin anion of the heteropolyoxometallate and TiO_2 surfaces producing composites or surface complexes [20,38].

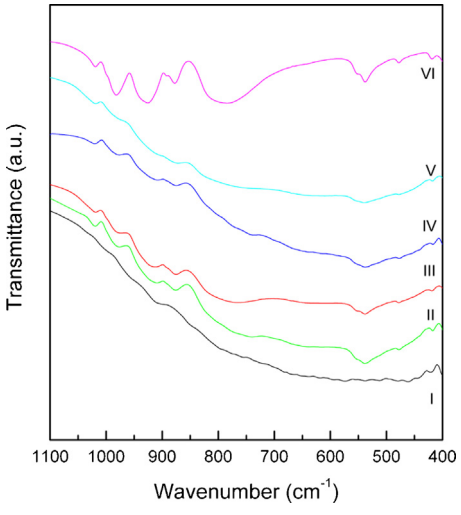

Fig. 2. FT-IR spectra of $TiTSA00_{T100}$ (I), $TiTSA30_{T100}$ (II), $TiTSA30_{T600}$ (III), $TiTSA30_{T700}$ (IV), and $TiTSA30_{T800}$ (V) samples; bulk TSA (VI).

3.1.4. Diffuse reflectance UV–vis spectroscopy (DRS)

The UV–vis-DRS spectra of TiTSA00 samples presented intense absorption in the range 200–390 nm, corresponding to charge transfer from the valence band (O 2p) to the conduction band (Ti 3d) [42]. On the other hand, bulk TSA displayed two absorption bands in the range 200–450 nm, assigned to the charge transfer from bridging or terminal O 2p to W 5d (W–O–W and W–O_d, respectively) [43].

We have previously reported that modification the TiO_2 matrix with TPA leads to the materials with visible light absorption in the region 400–500 nm [17,38]. Herein DRS results revealed that the incorporation of TSA into TiO_2 also leads to visible light absorption; this light absorption was dependent on the temperature and TSA content. The TiTSA20 and TiTSA30 samples calcined at 500 and 600 °C showed high visible light absorption (Fig. 4). However, small changes in the 400–500 nm regions of the UV–vis-DRS spectra for the samples treated at 700 and 800 °C were detected and hence, the visible light absorption of these materials decreased.

The band gap energy of TiTSA00 samples calculated from the absorbance values of the DRS spectra was in the range 3.20–2.99 eV (Table 1). The values decreased when the calcination temperature increased, probably as a result of a higher crystallinity and the appearance of the rutile phase. For the TSA-modified titania samples, the E_g values slightly decreased in the following order: $TiTSA10_{T100} > TiTSA20_{T100} > TiTSA30_{T100}$ (Table 2), and they remained almost constant with the temperature increase.

In summary, the characterization of TiO_2 samples modified with TSA revealed that $[SiW_{12}O_{40}]^{4-}$ Keggin anion is the main species present in materials annealed at 500 and 600 °C. This

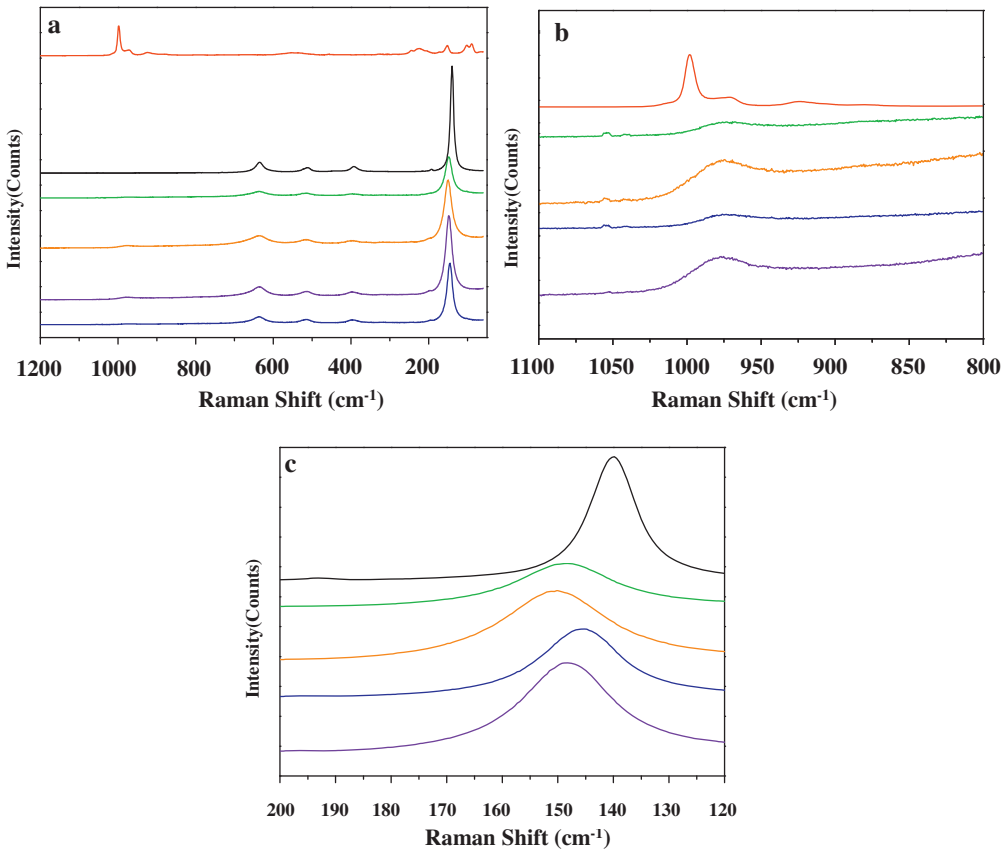

Fig. 3. Raman spectra of TSA ( ), TiTSA00$_{600}$ (—), TiTSA20$_{500}$ ( ), TiTSA30$_{500}$ ( ), TiTSA20$_{600}$ ( ), TiTSA30$_{600}$ ( ).

incorporation induced visible light absorption probably caused by a strong interaction of TSA Keggin anion and TiO_2 through the formation of composites or surface complexes. Moreover, the presence of TSA in TiO_2 increased the anatase–rutile phase transition temperature.

3.2. Photocatalytic activity

The photocatalytic activity of synthesized materials was tested in the photocatalytic degradation of 4-chlorophenol (4-CP) at pH 6.9. Under these experimental conditions, 4-CP (a weak acid,

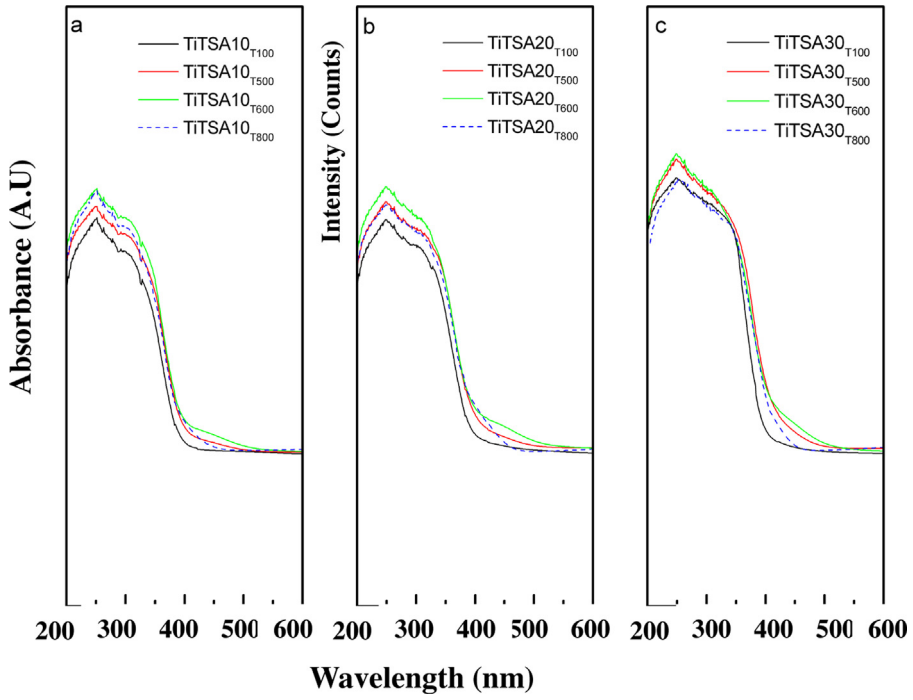

Fig. 4. UV–Vis-DRS spectra of TiTSA10 (a), TiTSA20 (b), and TiTSA30 (c) samples treated at 100, 500, 600, and 800 °C.

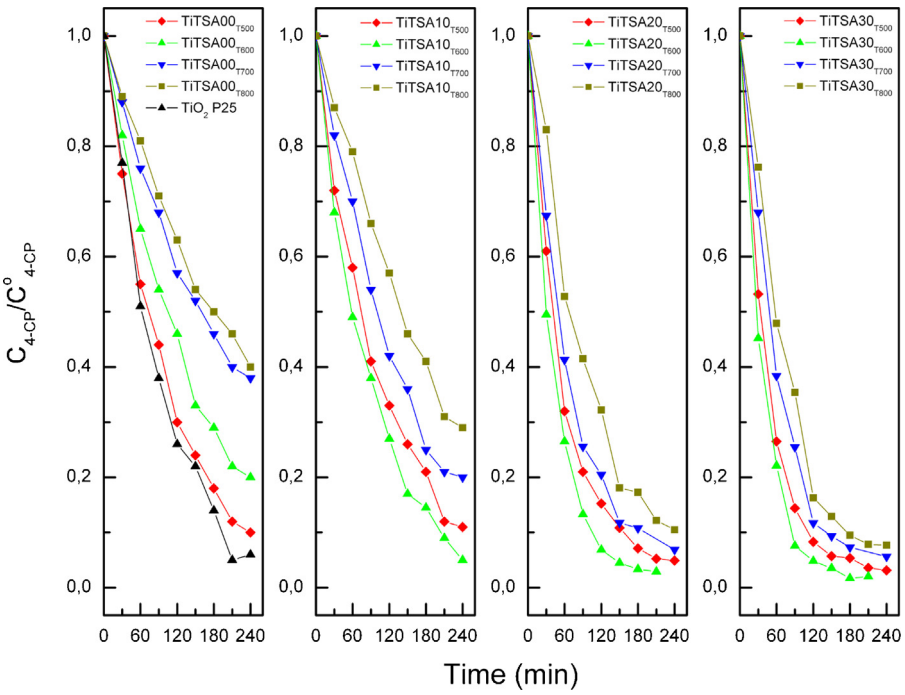

Fig. 5. Photocatalytic degradation of 4-CP as a function of the irradiation time for the TiTSA samples treated at 500, 600, 700, 800 °C, and TiO_2 Degussa P25.

p*Ka* = 9.41) was mainly present in the non-ionized form, and the surface of the catalysts was mostly negatively charged (pH_{pzc} of all TiTSA samples ranging between 2.8 and 5.2, see Table 2). As a result, 4-CP is not significantly adsorbed on the catalyst surface.

Photolysis experiments showed negligible 4-CP degradation after 240 min of irradiation. The reduction in the 4-CP concentration was lower than 9% at 240 min under reaction when $TiTSAxx_{T100}$ was used as catalyst.

The 4-CP degradation profiles using TiTSA00, TiTSA10, TiTSA20, and TiTSA30 samples calcined at temperatures in the range 500–800 °C are shown in Fig. 5. The results show that for TiTSA00 and TiTSAXX samples, the amount of 4-CP degraded after 240 min of light irradiation increased when the calcination temperature was raised up to 500 and 600 °C, respectively, and decreased at higher temperature values. Furthermore, when a particular temperature is considered, the amount of degraded 4-CP increased with the increment of the TSA content. Besides, for all the samples the 4-CP percentage degraded after 240 min was higher than those obtained using samples treated at 100 °C. The degradation profile of 4-CP using TiO_2 Degussa P25 (commonly used as reference) was very similar to those of the $TiTPA00_{500}$ and $TiTPA10_{500}$ samples.

As was reported in previous studies [44–46], results of photocatalytic activity were fitted using a pseudo-first-order kinetic model with respect to the 4-chlorophenol concentration considering that the reaction rate follows the Langmuir–Hinshelwood model:

$$r_{4\text{-CP}} = -\frac{dC_{4\text{-CP}}}{dt} = \frac{k_r K C_{4\text{-CP}}}{1 + K C_{4\text{-CP}}} \quad (1)$$

where $r_{4\text{-CP}}$ is the degradation rate, $C_{4\text{-CP}}$ is the 4-CP concentration, and k_r and K are the reaction and the adsorption constants, respectively. When $C_{4\text{-CP}}$ is low, $KC_{4\text{-CP}}$ is generally negligible and the reaction rate can be assumed as of pseudo-first-order with respect to the pollutant concentration. The resultant equation (2) can be integrated considering that $C_{4\text{-CP0}}$ is the 4-CP concentration at time equal zero.

$$\ln\left(\frac{C_{4CP0}}{C_{4\text{-CP}}}\right) = k_r K t \quad (2)$$

Apparent reaction constant $k_{ap} = k_r K$ values were obtained from the plots of $\ln(C_{4\text{-CP0}}/C_{4\text{-CP}})$ as a function of time. As we can see in Fig. 6, the k_{ap} values of the TiTSA00 sample increased when the calcination temperature was raised up to 500 °C, as a result of the higher crystallinity of the $TiTSA00_{T500}$ sample compared with that treated at 100 °C, and are slightly lower than the value estimated for TiO_2 Degussa P25 ($k_{ap} = 1.05 \times 10^{-2}$ min^{-1}). The transformation of anatase into rutile phase and the drop of S_{BET} are responsible for the decrease of k_{ap} observed for $TiTSA00_{T600}$, $TiTSA00_{T700}$, and $TiTSA00_{T800}$ samples [47] (Fig. 6).

Fig. 6 shows that the highest k_{ap} value was displayed by the sample with the highest TSA content calcined at 600 °C. These results can be explained by the fact that at 600 °C the samples mainly contain well-crystallized anatase phase and it is well known that anatase TiO_2 is the crystalline phase with higher photocatalytic activity [1,2,4]. On the other hand, increasing the TSA content might produce two main effects: high absorption of visible light and low e^-/h^+ recombination. The light source used in this study emits UV

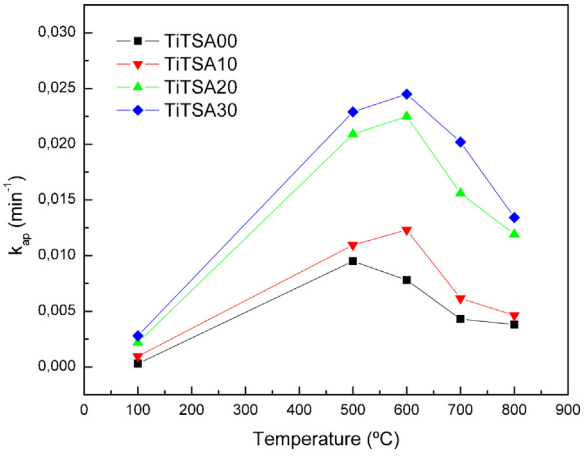

Fig. 6. Apparent reaction constant, k_{ap}, of 4-CP photocatalytic degradation as a function of the thermal treatment temperature.

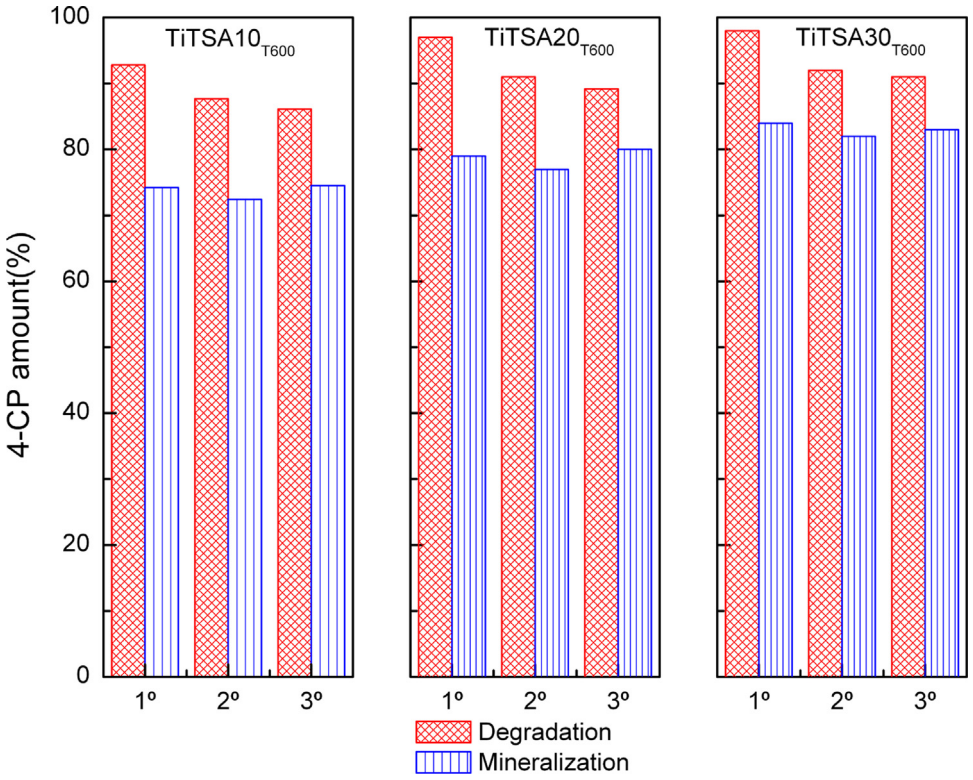

Fig. 7. 4-CP degradation and mineralization degree as a function of the number cycle of usage for the $TiTSA10_{T600}$, $TiTSA20_{T600}$, and $TiTSA30_{T600}$ catalysts.

and visible light, thus these photons could be exploited to yield charge carriers and participate in oxidation reactions. However the degradation of 4-chlorophenol may be mainly carried by UV light absorption, taking into account that when $TiTSA30_{T500}$ was irradiated using only blue light (wavelength in the range 400–500 nm; see supplementary data), 4-CP underwent a slight degradation (around 20%). Moreover, TSA Keggin anion ($[SiW_{12}O_{40}]^{4-}$) could easily accept photo-induced e_{CB}^- from TiO_2. The first redox potential of $[SiW_{12}O_{40}]^{4-}$ is −0.055 V vs. NHE [48] and at pH 6.9 the redox potential of TiO_2 e_{CB}^- is −0.52 V (vs. NHE) [2], thus electronic transfer from TiO_2 to $[SiW_{12}O_{40}]^{4-}$ would be thermodynamically favorable and the Keggin anion should behave as an electron sink decreasing the e^-/h^+ recombination and enhancing the photocatalytic activity of these materials.

The diminution in k_{ap} shown for the samples annealed at 700 and 800 °C could be assigned to the structure disruption of the $[SiW_{12}O_{40}]^{4-}$ anion during the thermal treatment, as was suggested based on FT-IR studies.

GC/MS measurements using $TiTSA30_{T600}$ as photocatalyst revealed that benzoquinone (BQ) was the predominant intermediate and only traces of hydroquinone (HQ) and 4-chloro-cathechol (4-CC) were detected. Many studies have reported the appearance of benzoquinone (BQ), hydroquinone (HQ) and 4-chlorocatechol (4-CC) as the predominant aromatic reaction intermediates during the photodegradation of 4-CP [49–51].

Mylonas and Papaconstantinou [52] and Yue et al. [53] found that hydroquinone and benzoquinone were the major intermediaries when 4-CP was photodegraded using polyoxometallates and silica-immobilized polyoxometallates, respectively.

According to Kormali et al. [54], some of the intermediates detected during the 4-CP photodegradation catalyzed by $[PW_{12}O_{40}]^{3-}$ were not found or were present as traces (HQ and 4-CC respectively) when TiO_2 was used. They suggest that this happens due to the photodegradation catalyzed by $[PW_{12}O_{40}]^{3-}$ essentially operated via •OH radicals, while holes and •OH radicals take part in the case of TiO_2 photocatalysis.

Taking into account the obtained results, the samples that showed the highest activity ($TiTSA10_{T600}$, $TiTSA20_{T600}$, and $TiTSA30_{T600}$) were chosen to do reuse tests. After each photocatalytic experiment, the solids were easily separated from the resulting suspension by decantation, washed with distilled water, dried at 70 °C and reused. It is important to note that separation of TiTSA materials was easier than with P25 offering an important advantage. It is well known that separation of TiO_2 nanoparticles from aqueous solutions is one of the main drawbacks of heterogeneous photocatalysis to eliminate waterborne pollutants.

The percentage of degraded 4-CP after each cycle of usage (Fig. 7) remains practically unchanged for the $TiTSA10_{T600}$ and $TiTSA20_{T600}$ samples. However, in the case of the $TiTSA30_{T600}$ sample, it decreases slightly during the first reuse, and then keeps constant. For all the tested samples, the mineralization degree is lower than the amount of degraded 4-CP, due to the formation of organic intermediates previously mentioned. It also decreases in the same way as the degradation of 4-CP after each cycle of usage. This decrease in photocatalytic activity was attributed to leaching of TSA from the fresh samples during the first photocatalytic test, which was established by atomic absorption spectrometry as less than 1% of the TSA content. According to these results, after the third use the catalytic performance of the $TiTSA20_{T600}$ and $TiTSA30_{T600}$ samples is practically the same.

4. Conclusions

Mesoporous anatase TiO_2 modified with tungstosilicic acid (TSA) was synthesized by sol–gel-type reactions using urea as a pore-forming agent. The specific surface area of the materials decreased when both the TSA amount and the calcination temperature increased. Incorporation of TSA increased the anatase–rutile

transition temperature. Furthermore, crystallite size increased with the calcination temperature, but lower values were obtained for higher TSA content. The Keggin structure of the $[SiW_{12}O_{40}]^{4-}$ anion remained intact only in the samples thermally treated until 500 °C. A partial degradation of the Keggin-type structure took place at higher temperatures. The presence of Keggin anion on TiO_2 led to visible light absorption possibly due to the formation of TSA–TiO_2 surface complexes or TSA/TiO_2 composites.

Materials containing TSA exhibited higher photocatalytic activity in the 4-chlorophenol degradation than neat TiO_2. According to the apparent reaction constant, estimated assuming pseudo-first-order kinetics, the photocatalytic activity depends on the TSA amount and the thermal treatment temperature. The solid containing 30% TSA and annealed at 600 °C showed higher photocatalytic activity. On the other hand, reused photocatalysts showed only a slight decrease in the degradation and mineralization of 4-chlorophenol, thus TiO_2 materials modified with tungstosilicic acid seem to be promising photocatalysts to destroy waterborne pollutants.

Acknowledgements

The authors thank E. Soto, L. Osiglio, and G. Valle, for their experimental help, and the financial support of National Scientific and Technical Research Council-Argentina (CONICET) (Project number: PIP 628) and National University of La Plata (UNLP) (Project number X-603).

Appendix A. Supplementary data

Supplementary data associated with this article can be found, in the online version, at http://dx.doi.org/10.1016/j.jphotochem.2014.05.014.

References

[1] A. Di Paola, E. García-López, G. Marci, L. Palmisano, A survey of photocatalytic materials for environmental remediation, J. Hazard. Mater. 211–212 (2012) 3–29.
[2] A. Fujishima, X. Zhang, D.A. Tryk, TiO_2 photocatalysis and related surface phenomena, Surf. Sci. Rep. 68 (2008) 515–582.
[3] J.A. Rengifo-Herrera, A.G. Rincón, C. Pulgarin, Waterborne *Escherichia coli* inactivation by TiO_2 photo-assisted processes: a brief overview, in: P. Pichat (Ed.), Photocatalysis and Water Purification: From Fundamentals to Recent Applications, Wiley-VCH Verlag GmbH & Co. KGaA, Weinheim, Germany, 2013, pp. 295–311.
[4] T. Berger, M. Sterrer, O. Diwald, E. Knozinger, D. Panayotov, T.L. Thompson, J.T. Yates, Light-induced charge separation in anatase TiO_2 particles, J. Phys. Chem. B 109 (2005) 6061–6068.
[5] J. Zhang, Y. Wu, M. Xing, S.A. Leghari, S. Sajjad, Development of modified N-doped TiO_2 photocatalyst with metals, non-metals, Energ. Environ. Sci. 3 (2010) 715–726.
[6] C.A. Emilio, M.I. Litter, M. Kunst, M. Bouchard, C. Colbeau-Justin, Phenol photodegradation on platinized-TiO_2 photocatalysts related with charge-carrier dynamics, Langmuir 22 (2006) 3606–3613.
[7] D. Mitoraj, H. Kisch, Surface modified titania visible light photocatalysts powders, Sol. St. Phenom. 162 (2010) 49–75.
[8] M. Anpo, M. Takeuchi, The design and development of highly reactive titanium oxide photocatalysts operating under visible light irradiation, J. Catal. 216 (2003) 505–516.
[9] C. Di Valentin, E. Finazzi, G. Pacchioni, A. Selloni, S. Livraghi, M.C. Paganini, E. Giamello, N-doped TiO_2: theory and experiment, Chem. Phys. 339 (2007) 44–56.
[10] J.A. Rengifo-Herrera, K. Pierzchala, A. Sienkiwicz, L. Forro, J. Kiwi, C. Pulgarin, Abatement of organics and *Escherichia coli* by N, S co-doped TiO_2 under UV and visible light. Implications of the formation of singlet oxygen ($^1O_2$) under visible light, Appl. Catal. B: Environ. 88 (2009) 398–406.
[11] M. Mrowetz, W. Bakerski, A.J. Colussi, M.R. Hoffmann, Oxidative power of nitrogen-doped TiO_2 photocatalysts under visible illumination, J. Phys. Chem. B 108 (2004) 17269–17273.
[12] T. Okuhara, N. Mizuno, M. Misono, Catalytic chemistry of heteropoly compounds, Adv. Catal. 41 (1996) 113–252.
[13] L.R. Pizzio, P.G. Vázquez, C.V. Cáceres, M.N. Blanco, Supported Keggin type heteropolycompounds for ecofriendly reactions, Appl. Catal. A: Gen. 256 (2003) 125–129.
[14] E. Papaconstantinou, Photochemistry of polyoxometallates of molybdenum and tungsten and/or vanadium, Chem. Soc. Rev. 18 (1989) 1–31.
[15] M. Nasr-Esfahani, M. Montazerozohori, M. Moghadam, I. Mohammadpoor-Baltork, S. Moradi, Transformation of thioamide compounds to corresponding amides using 12-tungstosilisic acid, Phosphorus Sulfur 185 (2010) 261–266.
[16] C. Chen, W. Zhao, P. Lei, J. Zhao, N. Serpone, Photosensitized degradation of dyes in polyoxometalate solution versus TiO_2 dispersions under visible-light irradiation: mechanistic implications, Chem. Eur. J. 10 (2004) 1959–1965.
[17] J.A. Rengifo-Herrera, M.N. Blanco, L.R. Pizzio, Photocatalytic bleaching of aqueous malachite green solutions by UV-A and blue-light-illuminated TiO_2 spherical nanoparticles modified by tungstophosphoric acid, Appl. Catal. B: Environ. 110 (2011) 126–132.
[18] C. Yu, J.C. Yu, W. Zhou, K. Yang, WO_3 coupled with P-TiO_2 photocatalysts with mesoporous structure, Catal. Lett. 140 (2010) 172–183.
[19] N. Lu, Y. Zhao, H. Liu, Y. Guo, X. Yuan, H. Xu, H. Peng, H. Qin, Design of polyoxometallate-titania composite film ($H_3PW_{12}O_{40}/TiO_2$) for the degradation of an aqueous dye Rhodamine B under the simulated sunlight irradiation, J. Hazard. Mater. 199–200 (2012) 1–8.
[20] Y. Yang, Q. Wu, Y. Guo, C. Hu, E. Wang, Efficient degradation of dye pollutants on nanoporous polyoxotugnstate–anatase composite under visible light irradiation, J. Mol. Catal. A: Chem. 225 (2005) 203–212.
[21] P. Ngaotrakanwiwat, S. Saitoh, Y. Ohko, T. Tatsuma, A. Fujishima, TiO_2–phosphotungstic acid photocatalysis systems with energy storage ability, J. Electrochem. Soc. 150 (2003) A1405–A1407.
[22] M.N. Blanco, L.R. Pizzio, Properties of mesoporous tungstosilicic acid/titania composites prepared by sol–gel method, Appl. Surf. Sci. 256 (2010) 3546–3553.
[23] S. Li, W. Yang, C. Li, Proceedings of the International Conference in Environmental Science and Computer Engineering, Wuhan, 2010.
[24] V.M. Fuchs, E.L. Soto, M.N. Blanco, L.R. Pizzio, Direct modification with tungstophosphoric acid of mesoporous titania synthesized by urea – templated sol–gel reactions, J. Colloid Interface Sci. 327 (2008) 403–411.
[25] H. Yang, D. Zhang, L. Wang, Synthesis and characterization of tungsten oxide-doped titania nanocrystallites, Mater. Lett. 57 (2002) 674–678.
[26] E. Ortiz-Islas, T. López, R. Gómez, M. Picquart, D.H. Aguilar, P. Quintana, Crystallinity effect in the textural properties of titania-TPA catalysts, Appl. Surf. Sci. 252 (2005) 853–857.
[27] N. Phonthammachai, T. Chairassameewong, E. Gulari, A.M. Jamieson, S. Wongkasemjit, Structural andrheological aspect of mesoporous nanocrystalline TiO_2 synthesized via sol–gel process, Microporous. Mesoporous. Mater. 66 (2003) 261–271.
[28] K.M.S. Khalil, T. Baird, M.I. Zaki, A.A. El-Samahy, A.M. Awad, Synthesis and characterization of catalytic titania via hydrolisis of titanium (IV) isopropoxide, Colloids Surf. A. 132 (1998) 31–44.
[29] M.N. Blanco, L.R. Pizzio, Influence of the thermal treatment on the physicochemical properties and photocatalytic degradation of 4-chlorophenol in aqueous solutions with tungstophosphoric acid-modified mesoporous titania, Appl. Catal. A: Gen. 405 (2011) 69–78.
[30] S. Eibl, B.C. Gates, H. Knozinger, Structure of Wox/TiO_2 catalysts prepared from hydrous titanium oxide hydroxide: Influence of preparation parameters, Langmuir 17 (2001) 107–115.
[31] X.-F. Yu, N.-Z. Wu, H.-Z. Huang, Y.-C. Xie, Y.-Q Tang, A study of the monolayer dispersion of tungsten oxide of anatase, J. Mater. Chem. 11 (2001) 3337–3342.
[32] S.M. Kumbar, G.V. Shanbhag, F. Lefebvre, S.B. Halligudi, Heteropoly acid supported on titania as solid acid catalyst in alkylation of *p*-cresol with *tert*-butanol, J. Mol. Catal. A- Chem. 256 (2006) 324–334.
[33] M.N. Blanco, L.R. Pizzio, Properties of mesoporous tungstosilisic acid/titania composites prepared by sol–gel method, Appl. Surf. Sci. 256 (2010) 3546–3553.
[34] M. Pelaez, P. Falaras, V. Likadimos, A.G. Kontos, A.A. De la Cruz, K. O'shea, D. Dyonysiou, Synthesis, structural characterization and evaluation of sol–gel based NF-TiO_2 films with visible light-photoactivation for the removal of microcystin-LR, Appl. Catal. B: Environ. 99 (2010) 378–387.
[35] G.R. Hearne, J. Zhao, A.M. Dawe, V. Pischedda, M. Mazza, M.K. Nieuwoudt, P. Kibasomba, O. Memraoui, J.D. Comins, High-pressure X-ray diffraction and Raman spectroscopy studies of the tetragonal spinel $CoFe_2O_4$, Phys. Rev. B 70 (2004), 134102-1–134102-10.
[36] D.P. Sawant, A. Pinu, S.P. Mirajkar, F. Levefebvre, K. Ariga, S. Anandan, T. Mori, C. Nishimura, S.B. Halligudi, Tungstophosphoric acid supported over zirconia in mesoporous channels of MCM-41 as catalyst in veratrole acetylation, J. Mol. Catal. A: Chem. 271 (2007) 98–108.
[37] V. Brahmkhatri, A. Patel, Synthesis and characterization of 12-tungstosilisic acid anchored to MCM-41 as well as its use as environmentally benign catalyst for synthesis of succinate and malonate diesters, Ind. Eng. Chem. Res. 50 (2011) 13693–13702.
[38] J.A. Rengifo-Herrera, M.N. Blanco, L.R. Pizzio, Visible light absorption of TiO_2 materials impregnated with tungstophosphoric acid-ethanol-aqueous solution at different pH values. Evidence about the formation of a surface complex between Keggin anion and TiO_2 surfaces, Mater. Res. Bull. 49 (2014) 618–624.
[39] G. Colon, M.C. Hidalgo, J.A. Navio, A. Kubacka, M. Fernndez-García, Influence of sulfur on the structural surface properties and photocatalytic activity of sulfated TiO_2, Appl. Catal. B: Environ. 90 (2009) 633–641.
[40] A.L. Bassi, D. Cattaneo, V. Russo, C.E. Bottani, E. Barborini, T. Mazza, P. Piseri, P. Milani, F.O. Ernst, K. Wegner, S.E. Pratsinis, Raman spectroscopy characterization of titania nanoparticles produced by flame pyrolysis: the influence of size and stoichiometry, J. Appl. Phys. 98 (2005), 074305-1–074305-9.

[41] J.C. Parker, R.W. Siegel, Calibration of the Raman spectrum to the oxygen stoichiometry of nanophase TiO_2, Appl. Phys. Lett. 57 (1990) 943–945.
[42] J.T. Yates, Photochemistry in TiO_2: mechanisms behind the surface chemistry, Surf. Sci. 603 (2009) 1605–1612.
[43] P.I. Villabrille, L.R. Pizzio, P.G. Vázquez, C.V. Cáceres, M.N. Blanco, Equilibrium adsorption of Keggin heteropolyacids on different supports, Curr. Top. Colloid Int. Sci. 6 (2003) 43–60.
[44] Y. Yang, Y. Guo, C. Hu, Y. Wang, E. Wang, Preparation of surface modification of mesoporous titania with monosubstituted Keggin units and their catalytic performance for organochlorine pesticide and dyes under UV irradiation, Appl. Catal. A: Gen. 273 (2004) 201–210.
[45] C. Lettmann, K. Hindenbrand, H. Kisch, W. Macyk, W.F. Maier, Visible light photodegradation of 4-chlorophenol with a coke-containing titanium dioxide photocatalyst, Appl. Catal. B: Environ. 32 (2001) 215–227.
[46] Y. Cheng, H. Sun, W. Jin, N. Xu, Photocatalytic degradation of 4-chlorophenol with combustion synthesized TiO_2 under visible light irradiation, Chem. Eng. J. 128 (2007) 127–133.
[47] C. Su, B.-Y. Hong, C.-M. Tseng, Sol–gel preparation and photocatalysis of titanium dioxide, Catal. Today 96 (2004) 119–126.
[48] P. Gómez-Romero, N. Casañ-Pastor, Photoredox chemistry in oxide clusters. Photochromic and redox properties of polyoxometalates in conexion with analog solid state colloidal systems, J. Phys. Chem. 100 (1996) 12448–12454.
[49] M.G. Kang, H.E. Han, K.J. Kim, Enhanced photodecomposition of 4-chlorophenol in aqueous solution by deposition of CdS on TiO_2, J. Photoch. Photobiol. A. 125 (1999) 119–125.
[50] X. Li, J.W. Cubbage, T.A. Tetzlaff, W.S. Jenks, Photocatalytic degradation of 4-chlorophenol. 1. The hydroquinone pathway, J. Org. Chem. 64 (1999) 8509–8524.
[51] N. Venkatachalam, M. Palanichamy, B. Arabindoo, V. Murugesan, Enhanced photocatalytic degradation of 4-chlorophenol by Zr^{4+} doped nano TiO_2, J. Mol. Catal. A: Chem. 266 (2007) 158–165.
[52] A. Mylonas, E. Papaconstantinou, On the mechanism of photocatalytic degradation of chlorinated phenols to CO_2 and HCl by polyoxometalates, J. Photoch. Photobiol. A. 94 (1996) 77–82.
[53] B. Yue, Y. Zhou, J. Yuxu, Z. Wu, X. Zhang, Y. Zou, S. Jin, Photocatalytic degradation of aqueous 4-chlorophenol by silica-immobilized polyoxometalates, Environ. Sci. Technol. 36 (2002) 1325–1329.
[54] P. Kormali, A. Troupis, T. Triantis, A. Hiskia, E. Papaconstatinou, Catal. Today 124 (2007) 149–155.